Appl. Phys. A 79, 1121–1125 (2004)
DOI: 10.1007/s00339-004-2659-1

Applied Physics A
Materials Science & Processing

N.N. NEDIALKOV[1]
P.A. ATANASOV[1,✉]
S.E. IMAMOVA[1]
A. RUF[2]
P. BERGER[2]
F. DAUSINGER[2]

Dynamics of the ejected material in ultra-short laser ablation of metals

[1] Institute of Electronics, Bulgarian Academy of Sciences, 72 Tsarigradsko Shose Blvd., Sofia 1784, Bulgaria
[2] Institut für Strahlwerkzeuge, Universität Stuttgart, Pfaffenwaldring 43, 70569 Stuttgart, Germany

Received: 15 September 2003/Accepted: 4 February 2004
Published online: 26 July 2004 •

ABSTRACT A molecular dynamics model is applied to study the formation and the early stages of ejection of material in ultra-short laser ablation of metals in vacuum. Simulations of the ablation process for iron at a pulse duration of 0.1 ps and at different laser fluences are performed. Different features of the ejection mechanism are observed below, near, and above the ablation threshold. The last is estimated as approximately 0.1 J/cm^2. The structure of the ablated material is found to depend on the applied laser fluence. The expanded plume consists mainly of large clusters at fluences near to the threshold. With the increase of the laser fluence the presence of the large clusters decreases. Clear spatial segregation of species with different sizes is observed in the direction normal to the surface several tens of picoseconds after the laser pulse onset. The angular distribution of the ejected material is estimated for different regimes of material removal. Above the ablation threshold the distribution is forward peaking.

PACS 79.20.Ds; 52.38.Mf; 02.70.Ns; 81.05.Bx

1 Introduction

Laser ablation is a basic process in a number of applications of lasers, such as micromachining, surface cleaning, surface-element analysis, generation of supersonic atomic and molecular beams, and pulsed laser deposition (PLD) of thin films and coatings. In many of these applications the properties of the ablated material, such as composition, velocity, and angular distribution of the ejected species, are critical. For example, the composition of the ablated material and the velocities of the particles in the plume strongly affect the quality, content of defects, and residual stresses of as-deposited thin films by PLD [1, 2].

Generally, the evolution of the ejected material can be divided schematically into two stages. The early stage includes a particle-removal process which is governed by the mechanism of ablation. In this stage the initial conditions of the plume are defined. In the second stage, the evolution of the ablated material comprises expansion, where the interaction between particles is most important. Many experimental [1, 3, 4] and theoretical [5–8] investigations have been devoted to the study of the properties of the laser-ablated plume in ultra-short laser ablation. The application of ultra-short laser pulses in the processing of materials reveals new possibilities and mechanisms for laser–solid interactions. Due to better spatial concentration of the energy, compared to nanosecond laser pulses, femto- and picosecond pulses ensure a lower ablation threshold. Furthermore, the interaction between ablated material and laser pulse can be neglected. The lower thermal losses compared to the nanosecond pulses cause smaller amounts of molten material and liquid droplets in the ablated plume. The ablation process with femtosecond pulses is also related to ejection of highly energetic particles, as their velocities can be one order of magnitude higher compared to the nanosecond regime [1]. Furthermore, it is shown [1] that, in femtosecond ablation, the lateral expansion of the plume is significantly smaller. The velocities of the ablated particles increase with rise of the laser fluence applied [3] and, depending on the composition and density of the plume, the velocity distribution can be described by a one-temperature shifted Maxwell–Boltzmann function or an elliptical (two-temperature) distribution [6]. Furthermore, depending on the laser fluence applied, the composition of the ablated material changes significantly, as it can contain fine clusters when the laser fluence is high enough above the threshold. On the contrary, relatively large portions of the material are expelled near to the threshold, as was shown for Cu [9]. The velocities of the ablated species and the expansion dynamics strongly depend on the kind and pressure of the background gas [1, 10]. Although some of the basic features of ultra-short laser ablation have been described and explained, the nature of the mechanisms of ejection is still unclear and needs further investigations.

In this work the early stage of the dynamics of the ultra-short laser-ablated plume is investigated on the basis of a molecular dynamics (MD) simulation. One of the main advantages of this method is that the interactions between particles and the dynamics of the different phases can be obtained without any considerations about the nature and the character of the processes involved.

2 Simulation details

The simulation model used in this work is based on the classical MD simulation technique [11]. The numerically stable and simple velocity Verlet algorithm is applied to in-

✉ Fax: +359-2/975-32-01, E-mail: gaslaser@ie.bas.bg

tegrate the equation of motion. The interaction between the atoms in the system is described by the Morse potential and its particular parameters for Fe are taken from [12]. In order to avoid the interaction between atoms at distances longer than the potential cutoff radius, the calculations are organized using the cell structure and the link-list method. The initial velocities are randomly ascribed to the atoms according to the Maxwell–Boltzmann distribution at room temperature. The modeled material is formed by certain numbers of unit face-centered-cubic cells in x, y, and z directions, respectively. The processes are investigated up to several tens of picoseconds.

The evolution of the ablation process is investigated in two configurations of the modeled system:

(i) Periodic boundary conditions for the atoms are applied in the x and y directions of the computational domain in order to simulate an infinite medium. This means that the processes occurring in the center of the laser spot are examined and effects of the edges of the laser spot are neglected. A velocity-dampening technique is applied at the bottom of the computational cell in order to prevent the artificial ablation effects that arise out of the shock-wave reflection from the bottom boundary of the system.

(ii) The laser pulse is focused at the center of the simulation system. It has a Gaussian spatial distribution of the intensity. This configuration of the system will provide a very precise description of the ablated plume expansion in the x–y plane.

The interaction is simulated for Fe at a pulse duration of $\tau_p = 0.1$ ps (FWHM) and a wavelength of $\lambda = 800$ nm. The optical parameters of the material used in the calculations at this wavelength are the reflectivity $R = 65\%$ and the absorption coefficient $\alpha = 0.54 \times 10^6\,\mathrm{cm}^{-1}$. The laser-beam intensity has a Gaussian temporal distribution and spatial uniformity in the first configuration and a Gaussian spatial distribution in the second. The ablation process in vacuum is studied.

2.1 *Absorption of the laser light*

A number of photons, corresponding to the laser energy, is deposited in the material exponentially following Lambert–Beer's law. The energy of the photons is transferred to the atoms of the system within a characteristic time τ_{eq}, corresponding to the time of electron–lattice energy transfer and the establishment of the equilibrium temperature. The time τ_{eq} depends on the properties of the material and it is between hundreds of femtoseconds and several tens of picoseconds in the case of metals [13, 14]. Based on the two-temperature diffusion model [15, 16], we have estimated this time to be about 5 ps for Fe.

The energy deposited to the atoms in the system contributes to the increase of their kinetic energy. The electron thermal diffusion is taken into account in the model by an increasing of the effective depth of the penetration of the laser energy. This depth is estimated from the electron thermal diffusion length $l_{th}^{e} \approx \left(D_e \tau_{eq}\right)^{1/2}$ (where $D_e = K_e/C_e$ is the electron diffusion coefficient), with the values of the electron thermal conductivity K_e and the electron heat capacity C_e estimated on the basis of [15–18].

Due to the limitations of the MD modeling in terms of number of particles, in the case of simulations with a Gaussian spatial distribution (ii), the laser pulse is focused in an area of several nanometers and the depth $1/\alpha$ and electron thermal diffusion length values are scaled down with a factor of 20. The scaling is also applied to the spatial distribution of the laser intensity. The deposited energy is estimated from the volume density of the photons corresponding to the real conditions.

3 Results and discussion

The experiments on ultra-short laser ablation of metals reported in our previous work [19] show that the ablation of metals can be divided into different regimes depending on the laser fluence applied. These regimes are expressed by different ablation rates (depth per pulse) at laser fluence rise. The MD model reveals that the change of the ablation rate is also related to a change of the mechanisms of ablation and the properties of the ablated material. At a laser fluence below approximately $F = 0.1\,\mathrm{J/cm}^2$ (we call this value the ablation threshold), the rate of material removal is up to several nanometers per pulse. The ablated material consists mainly of single particles produced by desorption.

Figure 1 represents snapshots of the evolution of the ablation process in Fe at $F = 0.15$ and $1.0\,\mathrm{J/cm}^2$, taken 7 ps after laser pulse onset for the case (ii). The increase of the laser fluence above the threshold results in an apparent rise of the amount of the ejected material. At $F = 0.15\,\mathrm{J/cm}^2$ (Fig. 1a) the deposited energy causes transient isochoric heating of the material, which is related to fast removal of material. The temperature on the surface is slightly above the evaporation temperature and one can assume that the intensive material removal is connected with the development of strong pressure in the absorbing volume. Since the deposited energy in depth is not sufficient to cause a transition into the gas phase, the ablated material consists of big and low-energetic clusters of molten material. Due to their low velocities and the collisions a significant part of the ablated material is re-deposited on the surface. The ablated crater has

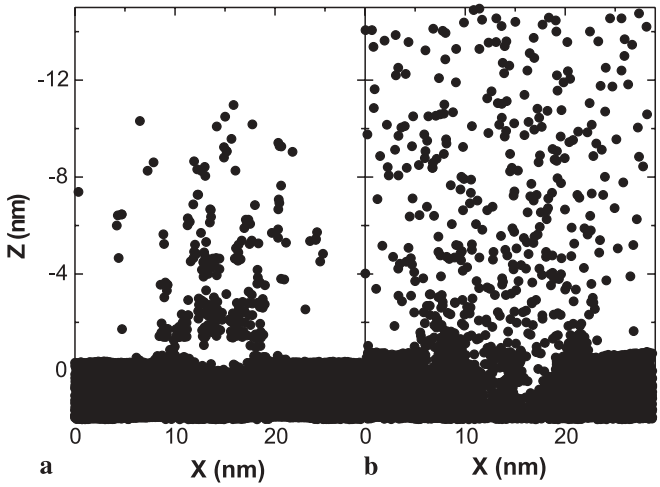

FIGURE 1 Snapshots of the evolution of the ablation process in Fe at $\tau_p = 0.1$ ps, taken at 7 ps after laser pulse onset. **a** $F = 0.15\,\mathrm{J/cm}^2$; **b** $F = 1\,\mathrm{J/cm}^2$

rough walls, and the presence of molten material remaining is negligible.

Further increase of the laser fluence changes considerably the features of the ablation and the properties of the ejected material (Fig. 1b). Here, presence of big clusters in the plume decreases. The time evolution of the average temperature of the particles in the absorbing volume for $F = 1\,\mathrm{J/cm^2}$ is shown in Fig. 2. As one can see, the material is rapidly overheated. This results in fast, explosion-like expansion of the heated volume. Several picoseconds later, the material starts to decompose into single particles, clusters, and liquid droplets. The process is accompanied by fast cooling of the overheated material, which is related to a transfer of the thermal energy into energy of decomposition.

A snapshot of the ablated plume, 20 ps after laser pulse onset, is presented in Fig. 3 at the conditions of Fig. 2 and the case (i). A detailed view of the structure of the ablated material is also presented for three different parts of the plume. As one can see, there is an apparent difference in the composition of the ejected material as a function of the distance from the surface. The top of the plume consists mainly of single particles, while small- and medium-sized clusters are observed in the middle part. In the region near the surface (lower part), the plume consists mainly of big clusters and droplets. This structure of the plume is related to the different degrees of heating of the material in depth.

Figure 4 represents the dependence of the average components V_z (normal to the surface) and V_{xy} (parallel to the surface) of the velocity of the ablated single particles on the distance from the surface (R_z) of the material taken at 25 ps after the laser pulse onset ($F = 1\,\mathrm{J/cm^2}$). As is seen, V_z can be described as a linear function of R_z. The clusters in the expanding plume have V_z of the same range as those of the single particles with the same R_z. However, the big liquid droplets located near to the surface of the material have velocities about two times lower, compared to those of the single particles and small clusters situated at the same R_z. One can assume that, due to the low velocities and high densities of these droplets, they may coalescence into bigger ones.

No contribution of the forward ejection in the V_{xy} components is observed and their values do not depend on the distance from the surface. Their distribution can be well described by a Maxwell–Boltzmann function (Fig. 5) and they can be referred to as the thermal motion of the species in the plume [5, 6]. The number of big clusters and droplets in the simulations is not enough to ensure good statistics for the velocity distribution, but an estimation shows that their thermal motion can not be described with the same temperature as the single particles. Due to the difference in the masses of the big species and single particles the thermalization is not achieved up to the end of the simulation.

The increase of the laser fluence results in a rise of the velocities of the ablated particles. Figure 6 shows the dependence of V_z for the single particles in the top of the plume on the

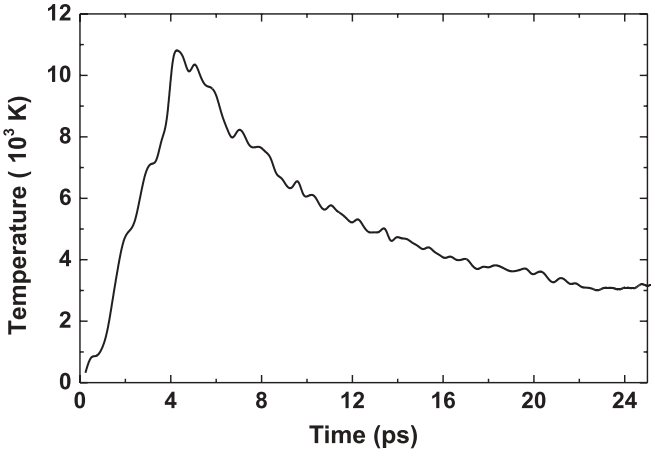

FIGURE 2 Time evolution of the average temperature of the particles in the absorbing volume. $F = 1\,\mathrm{J/cm^2}$ and $\tau_p = 0.1$ ps

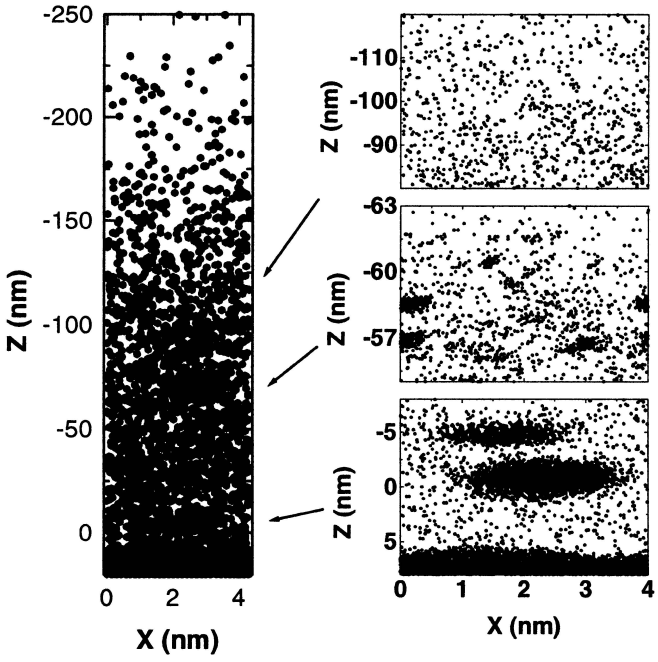

FIGURE 3 Snapshot of the ablated plume at 20 ps after laser pulse onset. $F = 1\,\mathrm{J/cm^2}$ and $\tau_p = 0.1$ ps. The *insets* represent more detailed views of the structure of the ablated material at three different distances from the surface

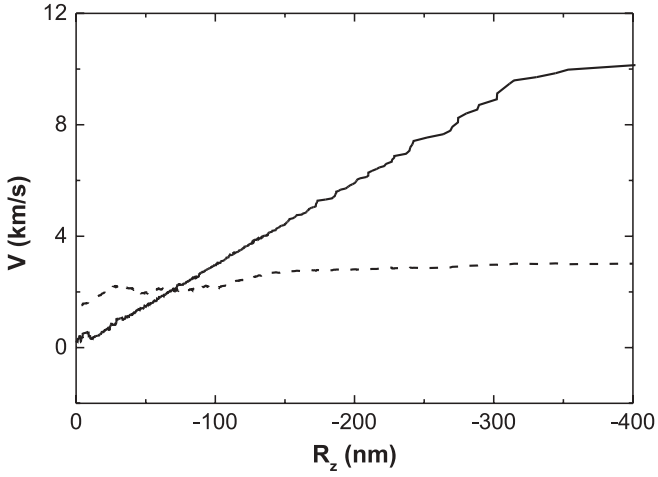

FIGURE 4 Dependence of the average normal (*solid curve*) and radial (*dashed curve*) velocity components of the ablated single particles on the distance from the surface, taken at 25 ps after laser pulse onset. $F = 1\,\mathrm{J/cm^2}$ and $\tau_p = 0.1$ ps

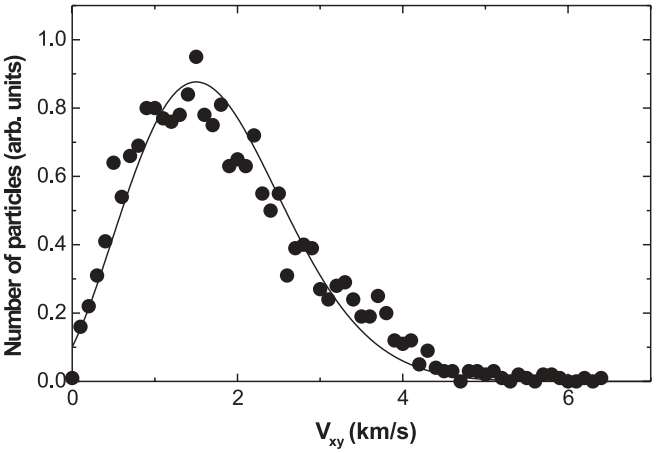

FIGURE 5 Distribution of the radial velocity components of the ablated single particles. The *dots* represent MD results; the curve is a Maxwell–Boltzmann distribution at $T = 10^4$ K. $F = 1\,\mathrm{J/cm^2}$ and $\tau_p = 0.1$ ps

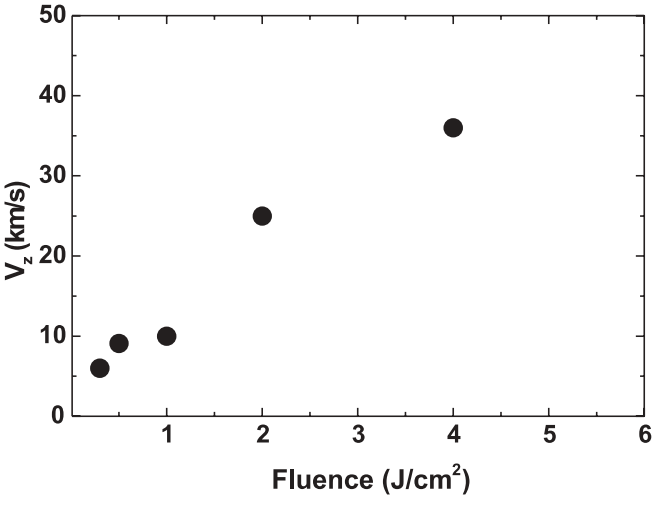

FIGURE 6 Dependence of the maximal normal velocity component (for the single particles at the top of the plume) on the laser fluence

laser fluence. These values are in acceptable agreement with the results found [1, 20, 21].

The ratio between the components of the particles' velocities (Fig. 4) indicates a forward peaking of the angular distribution of the plume. It is proposed [22] that the angular distribution of the ablated particles could be described by $\cos^p(\theta)$, where θ is the polar angle measured from the surface normal, and $p = (1 + M)^2$, where M is the Mach number. Figure 7 represents the angular distributions of the plume for ablation at $F = 0.1\,\mathrm{J/cm^2}$ and $F = 2\,\mathrm{J/cm^2}$, respectively, taken at 50 ps after laser pulse onset. In the desorption regime ($F = 0.1\,\mathrm{J/cm^2}$), where the number of ejected particles is low and the collisions between them are absent, the angular distribution can be described by $\cos(\theta)$. At higher F the collisions between the particles cause a sharpening of the plume, and the main part of the ablated material is confined in a cone with a full angle of 80°. The line in Fig. 7 represents the function $\cos^6(\theta)$. This value for the parameter p describes a supersonic expansion. As one can see a significant deviation from the $\cos^6(\theta)$ distribution is observed for the species expanded at big angles. This can be attributed to the fact that the $\cos^p(\theta)$ function describes the case where the plume is characterized

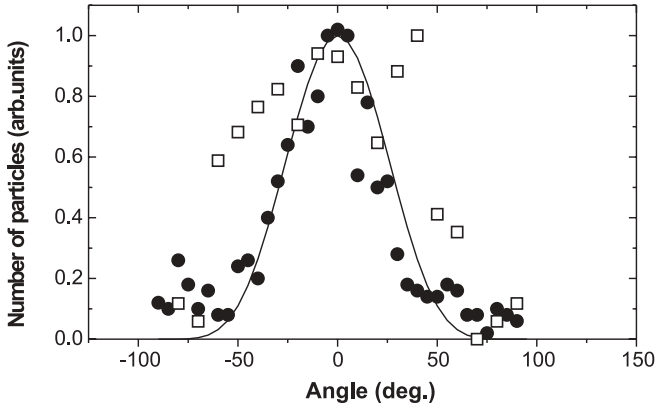

FIGURE 7 Angular distribution of the plume at 50 ps after the laser pulse onset. □ $F = 0.1\,\mathrm{J/cm^2}$; ● $F = 2\,\mathrm{J/cm^2}$. The *solid curve* represents the function $\cos^6(\theta)$

by a constant axial flow velocity. However, this is not the case here, as one can see from Fig. 4. About 100 ps later, the sharpening is more pronounced and the angular distribution can be approximated by $\cos^{10}(\theta)$. This sharpening is expressed mainly for particles in the upper part of the plume located near to the normal. The change of the laser spot size also affects the angular distribution of the ablated particles. A simulation performed with a four times higher diameter of the irradiated area at $F = 2\,\mathrm{J/cm^2}$ shows a sharpening of the ablated plume and the angular distribution can be described by $\cos^8(\theta)$ at 50 ps after laser pulse onset. A possible reason for this effect can be the increase of the number density of the particles in the plume and the rise of the number of collisions.

It should be mentioned that the formation of ions is not taken into account in the present model. Due to the repulsive action between them, one can expect that the plume tends to broaden in the early stage of its evolution. However, due to the presence of electrons in the plume, the interaction between the ions is restricted in space by the Debye screening length. Thus, the inclusion of the Coulomb interaction between the charged particles may weakly affect the plasma-expansion dynamics at a low degree of ionization. This is valid for the fluences used here. At higher laser fluence some non-thermal effects are expected to play a role in the ablation process [4]. Due to the Coulomb explosion and the ambipolar field effects, the ejected ions have higher energies.

4 Conclusions

In this work, a MD model is applied to investigate the process of formation and early stage of evolution of the plume in the femtosecond laser ablation of Fe. At laser fluences above the threshold of ablation (approximately $0.1\,\mathrm{J/cm^2}$) the ejection of the material is governed mainly by strong overheating of the absorbing volume. The ablated material consists of single particles, small and medium-sized clusters, and big droplets. Several tens of picoseconds after the laser pulse onset, spatial segregation of the different species in the plume is observed. Due to the decrease of the amount of the deposited energy in depth of the material, mainly single particles are located in the front of the plume, medium-sized clusters in the middle part, and big li-

quid droplets near to the surface. The clusters in the plume have the same velocities as the single particles at the same distance from the surface of the material. An exception is observed for the big liquid droplets. Due to the high difference in the masses of the single particles and the big droplets they are not thermalized up to the end of the simulations.

Due to the collisions between the particles the angular distribution of the plume is forward peaked. For the conditions of the present work it can be described as $\sim \cos^{10}(\theta)$.

ACKNOWLEDGEMENTS This work is supported financially in part by the BMBF Project No. 13N7710/6 (PRIMUS) of Germany and by the Bulgarian National Science Foundation under Contract No. F-1209.

REFERENCES

1 J. Perrière, E. Millon, W. Seiler, C. Boulmer-Leborgne, V. Craciun, O. Albert, J.C. Loulergue, J. Etchepare: J. Appl. Phys. **91**, 690 (2002)
2 A.V. Singh, R.M. Mehra, N. Buthrath, A. Wakahara, A. Yoshida: J. Appl. Phys. **90**, 5661 (2001)
3 M. Ye, C.P. Grigoropoulos: J. Appl. Phys. **89**, 5183 (2001)
4 Z. Zang, P.A. Van Rompay, J.A. Nees, P.P. Pronko: J. Appl. Phys. **92**, 2867 (2002)
5 L.V. Zhigilei: Appl. Phys. A **76**, 339 (2003)
6 M.I. Zeifman, B.J. Garrison, L.V. Zhigilei: J. Appl. Phys. **92**, 2181 (2002)
7 O. Ellegaard, J. Schou, H.M. Urbassek: Appl. Phys. A **69**, 577 (1999)
8 D. Sibold, H.M. Urbassek: Phys. Rev. A **43**, 6722 (1991)
9 E. Ohmura, I. Fukumoto: Int. J. Japan Soc. Precis. Eng. **30**, 128 (1996)
10 F. Garrelie, C. Champeaux, A. Catherinot: Appl. Phys. A **69**, S55 (1999)
11 M.P. Allen, D.J. Tildesley: *Computer Simulation of Liquids* (Clarendon, Oxford 1987)
12 I.A. Girifalco, V.G. Weizer: Phys. Rev. **114**, 687 (1959)
13 E.G. Gamaly, A.V. Rode, V.T. Tikhonchuk, B. Luther-Davies: Appl. Surf. Sci. **8094**, 1 (2002)
14 S.I. Anisimov, N.A. Inogamov, A.M. Oparin, B. Rethfeld, T. Yabe, M. Ogawa, V.E. Fortov: Appl. Phys. A **69**, 617 (1999)
15 S. Nolte, C. Momma, H. Jacobs, A. Tünnermann, B.N. Chichkov, B. Wellegehausen, H. Welling: J. Opt. Soc. B **14**, 2716 (1997)
16 K. Furusawa, K. Takahashi, H. Kumagai, K. Midorikawa, M. Obara: Appl. Phys. A **69**, 359 (1999)
17 B. Le Drogoff, F. Vidal, Y. von Kaenel, M. Chaker, T.W. Johnston, S. Laville, M. Sabsabi, J. Margot: J. Appl. Phys. **89**, 8247 (2001)
18 S.-S. Wellershoff, J. Hohlfeld, J. Güdde, E. Matthias: Appl. Phys. A **69**, 99 (1999)
19 N.N. Nedialkov, S.E. Imamova, P.A. Atanasov, G. Heusel, D. Breitling, A. Ruf, H. Hügel, F. Dausinger, P. Berger: Thin Solid Films **453–454**, 496 (2004)
20 R. Stoian, D. Ashkenasi, A. Rosenfeld, M. Wittmann, R. Kelly, E.E.B. Campbell: Nucl. Instrum. Methods Phys. Res. B **166–167**, 682 (2000)
21 E. Ohmura, I. Fukumoto, I. Miyamoto: in *Proc. ICALEO'98, Ser. A, 1998*, p. 45
22 R. Kelly, R.W. Dreyfus: Nucl. Instrum. Methods Phys. Res. B **32**, 341 (1988)